doi:10.1016/j.jmb.2009.11.023 J. Mol. Biol. (2010) 396, 130–140

JMB

Available online at www.sciencedirect.com

ScienceDirect

ELSEVIER

The Unique Kinetics of Iron Release from Transferrin: The Role of Receptor, Lobe–Lobe Interactions, and Salt at Endosomal pH

Shaina L. Byrne[1], N. Dennis Chasteen[2], Ashley N. Steere[1] and Anne B. Mason[1]*

[1]*Department of Biochemistry, College of Medicine, University of Vermont, 89 Beaumont Avenue, Burlington, VT 05405, USA*

[2]*Department of Chemistry, Parsons Hall, University of New Hampshire, Durham, NH 03824, USA*

Received 11 September 2009; received in revised form 4 November 2009; accepted 10 November 2009
Available online 13 November 2009

Transferrins are a family of bilobal iron-binding proteins that play the crucial role of binding ferric iron and keeping it in solution, thereby controlling the levels of this important metal. Human serum transferrin (hTF) carries one iron in each of two similar lobes. Understanding the detailed mechanism of iron release from each lobe of hTF during receptor-mediated endocytosis has been extremely challenging because of the active participation of the transferrin receptor (TFR), salt, a chelator, lobe–lobe interactions, and the low pH within the endosome. Our use of authentic monoferric hTF (unable to bind iron in one lobe) or diferric hTF (with iron locked in one lobe) provided distinct kinetic end points, allowing us to bypass many of the previous difficulties. The capture and unambiguous assignment of *all* kinetic events associated with iron release by stopped-flow spectrofluorimetry, in the presence and in the absence of the TFR, unequivocally establish the decisive role of the TFR in promoting efficient and balanced iron release from *both* lobes of hTF during one endocytic cycle. For the first time, the four microscopic rate constants required to accurately describe the kinetics of iron removal are reported for hTF with and without the TFR. Specifically, at pH 5.6, the TFR enhances the rate of iron release from the C-lobe (7-fold to 11-fold) and slows the rate of iron release from the N-lobe (6-fold to 15-fold), making them more equivalent and producing an increase in the net rate of iron removal from Fe_2hTF. Calculated cooperativity factors, in addition to plots of time-dependent species distributions in the absence and in the presence of the TFR, clearly illustrate the differences. Accurate rate constants for the pH and salt-induced conformational changes in each lobe precisely delineate how delivery of iron within the physiologically relevant time frame of 2 min might be accomplished.

Keywords: stopped-flow fluorescence; iron release kinetics; salt effect; iron release model

Edited by R. Huber

Introduction

Human serum transferrin (hTF)[1] is a bilobal ferric-iron-binding glycoprotein. The nearly homologous N-lobe and C-lobe are connected by a short peptide linker and are further divided into two subdomains (NI/NII and CI/CII). The subdomains come together to form an iron binding cleft within each lobe.[1,2] Diferric hTF preferentially binds to specific transferrin receptors (TFRs) on the cell surface at neutral pH.[3] The complex undergoes clathrin-dependent receptor-mediated endocytosis during which the clathrin-coated pit fuses with an

*Corresponding author. E-mail address: anne.mason@uvm.edu.

Abbreviations used: hTF, human serum transferrin; TFR, transferrin receptor; apohTF, iron-free transferrin; sTFR, soluble portion of the transferrin receptor; Mes, 4-morpholineethanesulfonic acid; EDTA, ethylenediaminetetraacetic acid; DMEM–F12, Dulbecco's modified Eagle's medium–Ham F-12 nutrient mixture; UG, Ultroser G; BHK, baby hamster kidney; KISAB, kinetically significant anion binding.

endocytic vesicle. The pH within the endosome is lowered to ~5.6, resulting in protonation of the synergistic carbonate anion and iron binding residues, which, in turn, loosens the cleft and facilitates iron release to an as yet unidentified chelator. At the low pH within the endosome, iron-free transferrin (apohTF) remains bound to the TFR and is recycled back to the cell surface. Upon exposure to the pH of serum (~7.4), the complex dissociates, and released apohTF is free to bind more iron and to repeat the cycle. Entry of hTF into the cell, removal of iron from hTF, and return to the surface are completed in ~2–3 min.[4,5] Because ferrous iron is transported out of the endosome by a divalent metal transporter, DMT1, there is a requirement for reduction of ferric iron (Fe^{3+}).[6] Discovery of a ferrireductase (Steap3) residing in the membrane of the endosome provided a means for accomplishing the reduction.[7] While the TFR is known to influence the redox potential of iron bound to hTF,[8] the weight of evidence indicates that Fe^{3+} is first released from diferric hTF and is then reduced by Steap3.[9]

Ferric iron is coordinated in a near-octahedral geometry by identical ligands in each lobe of hTF: two tyrosines, one histidine, one aspartic acid, and two oxygens from the synergistic carbonate anion, which, in turn, is anchored to a highly conserved arginine residue.[10] Although the iron binding ligands are identical, the precise steps leading to iron release from each lobe differ due largely to differences in "second-shell" residues that do not directly coordinate the iron but participate in an extended and intricate hydrogen-bonding network with the primary ligands.[11–13]

Two lysine residues lie on opposite sides of the iron binding cleft—Lys206 in the NII subdomain and Lys296 in the NI subdomain—and are 3.04 Å apart in the iron-bound isolated hTF N-lobe structure and 9 Å apart in the apo structure of this lobe; these residues comprise the "dilysine trigger."[12–14] They share a hydrogen bond at neutral pH that is protonated at low pH and literally triggers the opening of the cleft. In the C-lobe, Lys534 (in the CII subdomain) and Arg632 (in the CI subdomain) are found in positions homologous to those of Lys206 and Lys296, respectively.[14] Mutation of Lys206 to glutamate in the N-lobe or mutation of Arg632 to alanine in the C-lobe to form $Lock_N$hTF [recombinant diferric hTF that contains an N-terminal hexa-His tag and is nonglycosylated (mutation K206E locks iron in the N-lobe)] and $Lock_C$hTF [recombinant diferric hTF that contains an N-terminal hexa-His tag and is nonglycosylated (mutation R632A locks iron in the C-lobe)] constructs, respectively, completely prevents iron release from that lobe on a relevant timescale and allows targeted measurement of iron release from the opposite lobe.[15–17]

It is well established that the presence of salt affects the iron release properties of each lobe of hTF.[18] In fact, iron release requires binding of a nonchelating anion, such as Cl^-, to an anion binding site that is distinct from the synergistic anion binding site. Specifically, it has been suggested that residues termed KISAB (*ki*netically *s*ignificant *a*nion *b*inding) sites exist in each lobe of hTF.[19] To exert an effect, such anions must bind to a site (or to multiple sites) on the iron-loaded closed form of hTF. Ideally, the anion binding effect should also be pH sensitive; at neutral pH, it would exert a negative or retarding effect on iron release because it is highly desirable to retain iron until delivery within the endosome. Once iron is removed, anions may play a different role in which they bind to and stabilize the open conformation. This suggestion is substantiated by identification of sulfate binding sites in the N-lobe that are inaccessible in the iron-bound N-lobe; therefore, anions cannot exert any effect on them until the iron is removed.[20,21]

The rate of iron release from hTF can be measured by an increase in the intrinsic Trp fluorescence (with a small contribution from Tyr residues) that occurs upon iron removal. hTF has eight Trp residues: three in the N-lobe and five in the C-lobe. Ferric iron within each binding cleft strongly quenches Trp fluorescence through radiationless transfer of electronic excited-state energy.[22] This energy is transferred via a Tyr-to-Fe^{3+} charge transfer absorption band at 470 nm,[23] which overlaps the Trp fluorescence emission band. Additionally, the charge transfer band results in a disruption of the π-to-π^* transition energy of the liganding Tyr residues, leading to an increase in the UV absorbance overlapping the intrinsic Trp fluorescence.[22] The decrease in absorbance (at 470 nm) or the increase in fluorescence signal has been utilized to derive rate constants associated with the iron release process. The recovery of the intrinsic fluorescence signal from Trp (and, to a much smaller extent, Tyr) can be monitored as iron is removed from hTF. Additionally, the large conformational changes associated with iron removal impact specific Trp residues that are very sensitive to alterations in their local environment.[24,25] Thus, the increase in the intrinsic Trp signal is ascribed to a combination of unquenching by loss of iron, triggering the large conformational changes in hTF and more localized changes in the immediate environment of the Trp residues. Recent studies from our laboratory have determined the contributions of the individual Trp residues in each lobe to the iron release signal,[26,27] with no contribution from the 22 Trp residues in the dimer of the soluble portion of the transferrin receptor (sTFR; residues 121–760, expressed as a recombinant entity that contains an N-terminal hexa-His tag).[28]

Early studies by Bali *et al.*[29] and Bali and Aisen[30, 31] provided the first insights into the mechanistic role of TFR in iron removal from diferric hTF. A time-based steady-state fluorescence approach to monitoring iron release using the increase in the intrinsic Trp fluorescence from hTF was pioneered by the Aisen laboratory.[32] In their series of kinetic studies, iron release to the chelator pyrophosphate was measured with monoferric N-lobe and monoferric C-lobe, diferric, and mixed-metal transferrins, with kinetically inert Co^{3+} introduced into one lobe and with

Fe^{3+} introduced into the other lobe of the protein. Experiments were performed in the presence or in the absence of full-length TFR isolated from placenta and solubilized at pH 5.6 using detergent micelles. Despite the technical challenges of this work (assuring that the metal was in the assigned lobe and remained there during the experiment, the low yield of TFR from the placenta, the requirement of detergent for its solubilization, and the instability of TFR at pH 5.6), the authors were able to conclude that, in the absence of the TFR, iron is released from the N-lobe, followed by the C-lobe, and that binding to the TFR induced a switch in this order.[29–31] Iron release from both lobes was observed to occur at comparable rates on the seconds timescale.

More recently, el Hage Chahine and Pakdaman[33] and Hemadi *et al.*[34] carried out pH jump chemical relaxation studies at $4.3 \leq pH \leq 6.5$ in which iron was removed from diferric and monoferric C-lobe transferrins using acetate as competing ligand in the presence and in the absence of detergent-solubilized TFR from placenta. Contrary to the findings of the Aisen laboratory, it was concluded that iron is preferentially removed from the N-lobe in both instances. Moreover, in the presence of the receptor, a rapid kinetic event on a milliseconds timescale was assigned to removal of iron from the N-lobe, whereas a much slower kinetic event on a seconds timescale was assigned to removal of iron from the C-lobe.

In the present work, we have addressed these issues by exploiting recombinant technology, including site-directed mutagenesis, to produce Fe_2hTF (recombinant diferric hTF that contains an N-terminal hexa-Histag and is nonglycosylated), authentic monoferric constructs {in which iron can bind in only one lobe or the other: Fe_NhTF [recombinant monoferric N-lobe hTF (mutations Y426F and Y517F preclude iron binding in the C-lobe) that contains an N-terminal hexa-His tag and is nonglycosylated] and Fe_ChTF [recombinant monoferric C-lobe hTF (mutations Y95F and Y188F preclude iron binding in the N-lobe) that contains an N-terminal hexa-His tag and is nonglycosylated]} and diferric locked constructs (in which iron can be removed from only one lobe or the other: $Lock_N$hTF and $Lock_C$hTF), as well as the sTFR (eliminating the need for detergent), to allow an unambiguous assignment of events related to iron release from hTF. The use of a sensitive stopped-flow spectrofluorimeter has provided data with a high signal-to-noise ratio, allowing the observation of early kinetic events not previously detected using the less sensitive steady-state format. Precise fitting of progress curves was achieved with equations describing the kinetic processes occurring during iron removal. In addition to iron release, we were able to assign rate constants to conformational changes within the individual lobes of hTF, to interactions with the sTFR, and to salt effects. Building on our recent qualitative study of iron release from these constructs and a model presented for iron release from Fe_2hTF in the absence of the sTFR,[17] we now present a comprehensive model for iron release from Fe_2hTF in the presence of the sTFR that more fully describes this complicated system. We provide accurate rate constants and irrefutable evidence that a critical role of the sTFR is to balance the rates of iron release from both lobes so that removal from Fe_2hTF occurs efficiently during one cycle of endocytosis. We also offer a compelling argument for why hTF is bilobal. Although our findings are in general accord with the early studies of Bali *et al.*[29] and Bali and Aisen,[30,31] they are more comprehensive and provide valuable new insights into this complex system.

Results and Discussion

Kinetic curves

The normalized kinetic curves for each authentic monoferric and locked construct at pH 5.6 under our "standard conditions" [100 mM 4-morpholineethanesulfonic acid (Mes; pH 5.6), 300 mM KCl, and 4 mM ethylenediaminetetraacetic acid (EDTA)] are overlaid with the curve for iron release from Fe_2hTF ± sTFR (Fig. 1). These conditions were chosen to simulate the putative endosomal pH. Because it is well established that salt affects the process, we arbitrarily chose a salt concentration (although, as detailed below, we assessed the effect of different concentrations of salt on the kinetic process). The chelator EDTA was chosen due to its stability and affinity for ferric iron at pH 5.6. A single concentration of EDTA was selected to provide a large excess, allowing us to maintain pseudo-first-order conditions in all experiments. It is important to remember that we are monitoring the increase in the intrinsic Trp fluorescence signal upon iron release and that both the unquenching of Trp residues as a result of iron removal and changes in the local environment of the three Trp residues in the N-lobe and of the five Trp residues in the C-lobe are observed. In fact, we have shown that only Trp128 and Trp264 in the N-lobe make significant contributions to the signal.[26] Likewise, in the C-lobe, the contributions are not uniform, with Trp460 in the cleft being the major contributor to the fluorescent signal.[27] Although the sTFR does not contribute to the *change* in the fluorescent signal upon release of Fe^{3+} from hTF, binding of hTF to the sTFR results in a significant decrease in the magnitude of the signal.[28]

As shown in Fig. 1, there are striking differences with regard to the shapes of the kinetic curves and their time courses for completion. Of great interest is the effect that the sTFR has on the iron release process (Fig. 1a and b *versus* Fig. 1c and d). Although significant differences are obvious simply from a visual comparison of the progress curves for the various constructs, quantitative information can only be derived from an accurate fitting of the data, as detailed below.

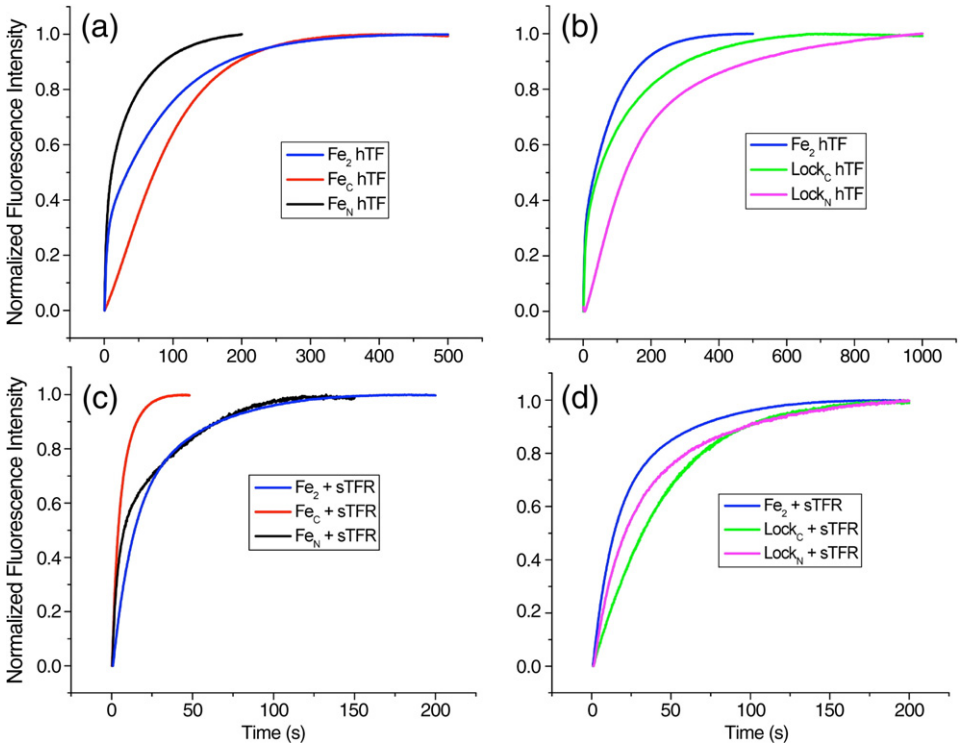

Fig. 1. Representative normalized stopped-flow fluorescence iron release progress curves in the presence and in the absence of the sTFR. (a) Overlay of Fe_NhTF, Fe_ChTF, and Fe_2hTF. (b) Overlay of $Lock_NhTF$, $Lock_ChTF$, and Fe_2hTF. (c) Overlay of Fe_NhTF/sTFR, Fe_ChTF/sTFR, and Fe_2hTF/sTFR. (d) Overlay of $Lock_NhTF$/sTFR, $Lock_ChTF$/sTFR, and Fe_2hTF/sTFR. In each experiment, one syringe contained protein (375 nM) in 300 mM KCl and the other contained iron removal buffer [200 mM Mes (pH 5.6), 300 mM KCl, and 8 mM EDTA]. Samples were excited at 280 nm, and emission was monitored using a 320-nm cut-on filter; the temperature was set at 25 °C.

Kinetic scheme

As established many years ago,[31,35] the stepwise removal of iron from Fe_2hTF to form monoferric transferrins and apohTF (in the absence and in the presence of the sTFR) depends on four microscopic rate constants k_{1N}, k_{1C}, k_{2N}, and k_{2C}, according to Scheme 1. Expressions have been developed for the time dependence of the concentrations of all four species and for the fluorescence intensity change measured in the stopped-flow experiments. Equations (1)–(4) in Table 1 represent the final integrated rate laws for the concentrations of Fe_2hTF, Fe_ChTF, Fe_NhTF, and apohTF as a function of time, where $[Fe_2hTF]_0$ is the initial concentration of Fe_2hTF. The derivation of these equations is provided in Supplemental Data. Substitution of the concentrations [Eqs. (2), (3), and (4)] into Eq. (5) (Table 1) provides the final kinetic expression for the change in fluorescence intensity as iron is removed.

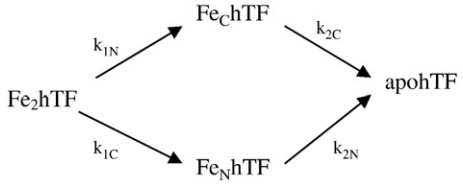

Scheme 1. Pathways of iron release from diferric hTF in the absence of the TFR.

Additionally, the kinetics of the constructs utilized to isolate k_{1N} ($Lock_ChTF$), k_{1C} ($Lock_NhTF$), k_{2N} (Fe_NhTF), and k_{2C} (Fe_ChTF) were fitted to standard consecutive reaction models (A→B, A→B→C, or A→B→C→D), as detailed in Supplemental Data, where examples of curve fitting of the data are also provided (Figs. S1–S3).

Kinetic assessment of iron release and conformational changes (no sTFR)

The rate constants presented in Fig. 2a are based on an analysis of the curves in Fig. 1a and b and are summarized in Table S1a. By using authentic locked and monoferric constructs (indicated below the arrows) along with the Fe_2hTF data, we can specifically assign the rate constants k_{1N}, k_{2N}, k_{1C}, and k_{2C} for each iron removal step, as well as rate constants reflecting conformational changes. The assignment of rate constants to iron removal steps is predicated on the reasonable assumption that they should have very similar values for a given lobe of the diferric, monoferric, and locked constructs. In no case is the assignment ambiguous when this criterion is applied (see Table S1a and b).

In the absence of the sTFR, curve fitting of the Fe_2hTF data indicates that iron is almost exclusively released first from the N-lobe ($k_{1N} = 17.7 \pm 2.2\ min^{-1}$) and then slowly from the C-lobe ($k_{2C} = 0.65 \pm 0.06\ min^{-1}$); that is, ~96% (= $\frac{k_{1N}}{k_{1N} + k_{1C}} \times 100$) of the

Table 1. Integrated rate equations

$$[Fe_2hTF]=[Fe_2hTF]_0 e^{-(k_{1N}+k_{1C})t} \quad (1)$$

$$[Fe_ChTF] = \frac{k_{1N}[Fe_2hTF]_0}{k_{2C}-k_{1N}-k_{1C}}\left(e^{-(k_{1N}+k_{1C})t} - e^{-k_{2C}t}\right) \quad (2)$$

$$[Fe_NhTF] = \frac{k_{1C}[Fe_2hTF]_0}{k_{2N}-k_{1N}-k_{1C}}\left(e^{-(k_{1N}+k_{1C})t} - e^{-k_{2N}t}\right) \quad (3)$$

$$[apohTF]=[Fe_2hTF]_0\left\{1-\left(1+\frac{k_{1N}}{k_{2C}-k_{1N}-k_{1C}}+\frac{k_{1C}}{k_{2N}-k_{1N}-k_{1C}}\right)e^{-(k_{1N}+k_{1C})t}+\frac{k_{1N}}{k_{2C}-k_{1N}-k_{1C}}e^{-k_{2C}t}+\frac{k_{1C}}{k_{2N}-k_{1N}-k_{1C}}e^{-k_{2N}t}\right\} \quad (4)$$

$$F(t) = F_C[Fe_ChTF] + F_N[Fe_NhTF] + F_{apo}[apohTF] \quad (5)$$

The change in fluorescence intensity $F(t)$ as a function of time is related to the time-dependent concentrations through Eq. (5), in which F_C, F_N, and F_{apo} are the molar fluorescence intensity constants for monoferric hTFs and apohTF, respectively.

iron is removed from the diferric protein through the upper kinetic pathway of Fig. 2a. [Note that inclusion of the rate constants for conformational transitions in fitting equations for the kinetic data for Fe_2hTF does not result in any significant changes in the values obtained for the rate constants k_{1N} and k_{2C} (Supplemental Data).]

The above assignment of rate constants for Fe_2hTF is confirmed by an analysis of the data from the $Lock_ChTF$ and Fe_ChTF constructs, which provide independent measures of k_{1N} and k_{2C}, respectively. The $Lock_ChTF$ data best fit an A→B→C→D model, giving three rate constants $k_1=k_{1N}=17.9\pm 3.1$ min^{-1} (*versus* $k_{1N}=17.7$ min^{-1}

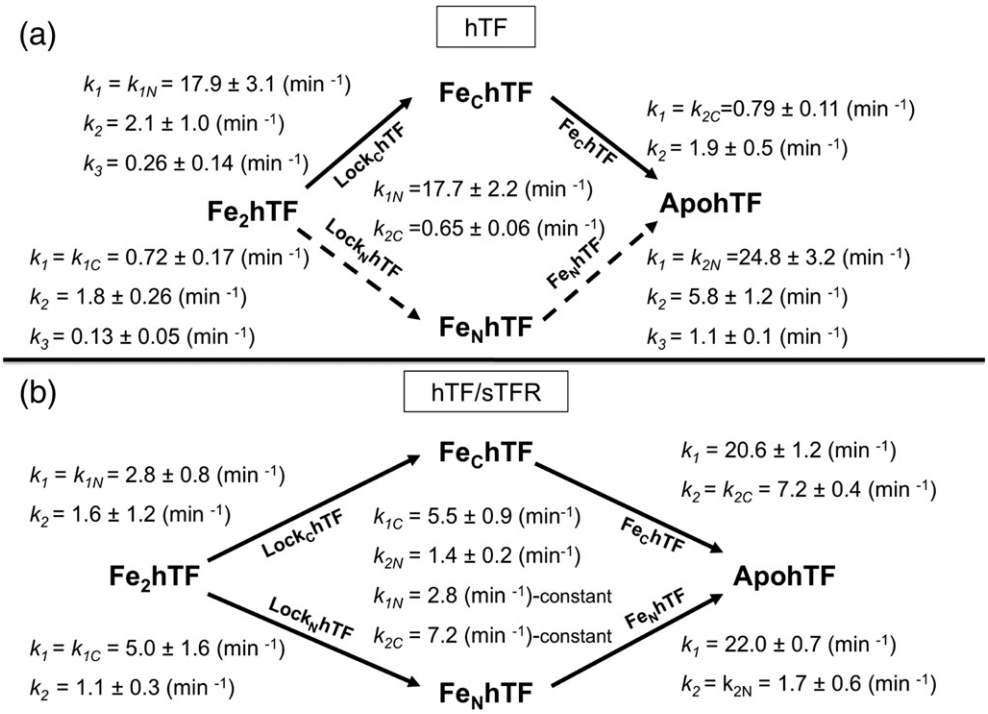

Fig. 2. Pathways of iron release±sTFR. (a) Iron release pathways of Fe_2hTF in the absence (b) and in the presence of sTFR. The primary pathways taken are indicated by continuous black arrows; the alternative pathway is indicated by broken black arrows. The specific construct used to isolate the rate constants is indicated below the arrows. Rate constants±errors at the 95% confidence level from multiple kinetic runs were obtained from the curve fitting of the data to models described in the text and in Supplemental Data and are indicated for each construct. In (b), k_{1N} (=2.8 min^{-1}) and k_{2C} (=7.2 min^{-1}) were held fixed at the values for $Lock_ChTF$ and Fe_ChTF, respectively, during fitting of the Fe_2hTF/sTFR data (see Supplemental Data).

for Fe_2hTF), $k_2 = 2.1 \pm 1.0$ min^{-1}, and $k_3 = 0.26 \pm 0.14$ min^{-1}, with the first assigned to iron release from the N-lobe and with the latter two assigned to sequential conformational changes within the N-lobe, ultimately leading to its final open apo conformation. Similar conformational changes are also observed for the N-lobe of Fe_NhTF and the isolated N-lobe (see the text below). The kinetics for Fe_ChTF fit an A → B → C model, with $k_1 = k_{2C} = 0.79 \pm 0.11$ min^{-1} for iron release (*versus* $k_{2C} = 0.65$ min^{-1} for Fe_2hTF) and one additional C-lobe event ($k_2 = 1.9 \pm 0.5$) ascribed to a structural adjustment to the final apo conformation, an event also observed with the C-lobe of $Lock_N$hTF and the isolated C-lobe (see the text below).

The rate constants determined for the $Lock_N$hTF and $Lock_C$hTF constructs provide further convincing support for the proposed order of iron release. If the alternative (lower) pathway (Fig. 2a, broken black arrows) were followed, then the rate constant k_{1C} for iron release from the C-lobe of $Lock_N$hTF would have been faster than the rate constant k_{1N} for iron release from the N-lobe of $Lock_C$hTF, but the opposite was true ($k_{1C} = 0.72$ min^{-1} *versus* $k_{1N} = 17.9$ min^{-1}).

The $Lock_N$hTF data were fitted to the A → B → C → D model, providing three rate constants, with the first being $k_1 = k_{1C} = 0.72 \pm 0.17$ min^{-1}, which corresponds very well to the rate of iron release from Fe_ChTF ($k_1 = k_{2C} = 0.79 \pm 0.11$ min^{-1}) and Fe_2hTF ($k_{2C} = 0.65 \pm 0.06$ min^{-1}). Similar to $Lock_C$hTF, iron release from the C-lobe of $Lock_N$hTF is followed by two conformational events, with $k_2 = 1.8 \pm 0.26$ min^{-1} and $k_3 = 0.13 \pm 0.05$ min^{-1}. We note that the rate constants corresponding to these conformational events have similar values in both $Lock_N$hTF and $Lock_C$hTF, namely, $k_2 = 1.8$ min^{-1} and $k_3 = 0.13$ min^{-1} *versus* $k_2 = 2.1$ min^{-1} and $k_3 = 0.26$ min^{-1}.

The kinetic data for Fe_NhTF indicate an initial fast step corresponding to iron release from the N-lobe ($k_1 = k_{2N} = 24.8 \pm 3.2$ min^{-1}), followed by two slower conformational events within the N-lobe ($k_2 = 5.8 \pm 1.2$ min^{-1} and $k_3 = 1.1 \pm 0.1$ min^{-1}). The rates of the final conformational change to the apo conformation are similar for the two monoferric constructs Fe_NhTF and Fe_ChTF (i.e., $k_3 = 1.1 \pm 0.1$ min^{-1} *versus* 1.9 ± 0.5 min^{-1}).

To further solidify the assignments and to elucidate the contribution of the lobe–lobe interaction to kinetics, we determined the rate constants for the isolated N-lobe and C-lobe (i.e., the two half-molecules of hTF). Data from the isolated N-lobe fit best to the A → B → C → D model, yielding three rate constants, with the first $k_1 = k_N = 53.7 \pm 3.3$ corresponding to iron removal and with the other two, $k_2 = 7.2 \pm 1.1$ min^{-1} and $k_3 = 1.2 \pm 0.6$ min^{-1}, corresponding to conformational events, as previously noted for the N-lobes of Fe_NhTF and $Lock_C$hTF, with the last event being the transition to the final apo N-lobe conformation. In contrast, data from the isolated C-lobe fit best to the A → B → C model, yielding two rate constants $k_1 = k_C = 0.87 \pm 0.10$ min^{-1} and $k_2 = 1.8 \pm 0.6$ min^{-1}, which are essentially identical with $k_1 = k_{2C} = 0.79$ min^{-1} and $k_2 = 1.9$ min^{-1} for the C-lobe of Fe_ChTF.

As previously discussed,[36] iron release from the N-lobe is substantially faster than iron release from the C-lobe ($k_N = 53.7$ min^{-1} *versus* $k_C = 0.87$ min^{-1}). Additionally, comparison of the rate of iron release from the isolated N-lobe to that from the full-length constructs reveals that the presence of the C-lobe substantially slows (3-fold) the rate of iron release from the N-lobe ($k_N = 53.7$ min^{-1} *versus* $k_{1N} = 17.9$ min^{-1}). In contrast, the rate constant for iron release from the C-lobe is essentially the same in the presence or in the absence of the N-lobe ($k_C = 0.87$ min^{-1} *versus* $k_{1C} = 0.72$ min^{-1}). This observation is in agreement with our previous qualitative data, which showed that iron release from the N-lobe in the absence of the receptor was impacted by the conformation of the C-lobe, whereas iron release from the C-lobe was not affected by the conformation of the N-lobe.[37] The kinetic cooperativity factors $k_{2N}/k_{1N} = 24.8/17.9 = 1.4$ and $k_{2C}/k_{1C} = 0.79/0.72 = 1.1$, which reflect the effect of the occupancy of the other lobe on the rate constant, also substantiate this assertion. These factors indicate that iron is removed more quickly from the N-lobe when the C-lobe is unoccupied, whereas occupancy of the N-lobe has little effect on the rate of iron release from the C-lobe.

Kinetic assessment of iron release and conformational changes from hTF/sTFR complexes

The rate constants presented in Fig. 2b are based on an analysis of the curves in Fig. 1c and d and are summarized in Table S1b. Their assignments follow a rationale similar to that presented above. Complete details are provided in the Supplemental Data.

Under our standard conditions, the kinetic data for iron release support previous work showing that the sTFR induces a switch in the order of iron release, such that the C-lobe preferentially releases its iron, followed by the N-lobe (Fig. 2b, lower pathway).[30,31] However, although analysis of the data in Fig. 2b corroborates this assertion, the situation is more complex. Thus, the fits indicate that iron release through the upper pathway of Fig. 2b is reduced from 96% in the absence of receptor to approximately 35% in its presence. Therefore, it is apparent that both the upper pathway and the lower pathway play important roles in the efficient removal of iron from Fe_2hTF in the presence of sTFR.

Based on the data for $Lock_N$hTF and Fe_ChTF, an ~7-fold to 11-fold increase in the rate constant for iron release from the C-lobe is observed in the presence of sTFR ($k_{1C,complex} = 5.0$ min^{-1} *versus* $k_{1C,alone} = 0.72$ min^{-1} and $k_{2C,complex} = 7.2$ min^{-1} *versus* $k_{2C,alone} = 0.79$ min^{-1}). Furthermore, based on the $Lock_C$hTF and Fe_NhTF data, there is a 6-fold to 15-fold *decrease* in the rate constant for iron release from the N-lobe upon binding of hTF to the sTFR ($k_{1N,complex} = 2.8$ min^{-1} *versus* $k_{1N,alone} = 17.9$ min^{-1} and $k_{2N,complex} = 1.7$ min^{-1} *versus* $k_{2N,alone} = 24.8$ min^{-1}). These differences are completely consistent with the rate constants that we have determined for iron release from Fe_2hTF (Fig. 2; Table S1) and recently published urea gel

data showing that binding to the receptor changes the order of iron release from the two lobes.[37] Importantly, the two rate constants for iron release from each lobe (k_{1C} *versus* k_{1N} and k_{2C} *versus* k_{2N}) are closer to each other in the presence of the sTFR than in its absence. For example, in the absence of the sTFR, iron release from the N-lobe is ~25 times faster ($=k_{1N,alone}/k_{1C,alone}$) than iron release from the C-lobe; however, in the presence of the sTFR, iron release from the C-lobe is only ~2 times faster ($=k_{1C,complex}/k_{1N,complex}$) than that from the N-lobe and similarly for k_{2C} and k_{2N}, indicating a leveling of rates. Thus, because binding to the TFR balances the rate of iron release from the two lobes, both pathways become important in the release of iron from hTF. As indicated by the cooperativity factors, the cooperativity between the lobes in iron release is also significantly affected by the binding to the sTFR [i.e., $(k_{2N}/k_{1N})_{alone}=1.4$ and $(k_{2C}/k_{1C})_{alone}=1.1$ *versus* $(k_{2N}/k_{1N})_{complex}=0.61$ and $(k_{2C}/k_{1C})_{complex}=1.5$]. Therefore, in the presence of the sTFR, the effect of the occupancy of the C-lobe on the release of iron from the N-lobe is reversed from what it was in its absence. Moreover, in the presence of the sTFR, the occupancy of the N-lobe retards the rate of iron release from the C-lobe, whereas in its absence, N-lobe occupancy had little influence on the kinetics of the C-lobe.

It was previously reported that the TFR has little effect on iron release from the monoferric N-lobe;[30] however, this earlier study captured only a single global kinetic event. Subsequently, a small decrease in the rate of iron release from the N-lobe of hTF, with Co^{3+} bound in the C-lobe, was reported.[31] In our work, even though it *appears* that k_1 values from Fe_NhTF alone and in complex with the sTFR are equal, as described in Supplemental Data, they can be confidently assigned to different events (Fig. 2).

Unfortunately, it is not possible to measure iron release from the isolated lobes bound to the sTFR because the isolated N-lobe does not bind at all to the sTFR[38,39] and the isolated C-lobe binds only weakly.[40] This is another indication that *both* lobes are required to achieve physiologically significant binding to the sTFR and that this binding tends to balance iron release from each.

The pronounced effect of the sTFR on iron release from the Fe_2hTF is most clearly appreciated from the time-dependent species distribution diagrams shown in Fig. 3. Figure 3a shows the species profile in the absence of the TFR. Iron is first rapidly lost from the N-lobe ($k_{1N}=17.7\ min^{-1}$) to form Fe_ChTF, which then only slowly releases its iron ($k_{2C}=0.65\ min^{-1}$) in the rate-limiting step to form apohTF. Little iron (~4%) is released from the C-lobe first ($k_{1C}=0.72\ min^{-1}$) to form a small amount of Fe_NhTF, which then rapidly decays ($k_{2N}=24.8\ min^{-1}$) to apohTF (Fig. 3a). In the absence of the sTFR, the time for 95% of the iron to be removed from the protein is 4.7 min (Fig. 3a), whereas in its presence, this time is reduced to 2.0 min (Fig. 3b)—a time well within the 2–3 min required for one cycle of endocytosis.[4,5] The role of both pathways in the enhanced net rate of iron removal in the Fe_2hTF/sTFR complex is further illustrated inFig. 3b, where the formation and decay of significant amounts of both Fe_NhTF and Fe_ChTF intermediates in the two pathways are evident.

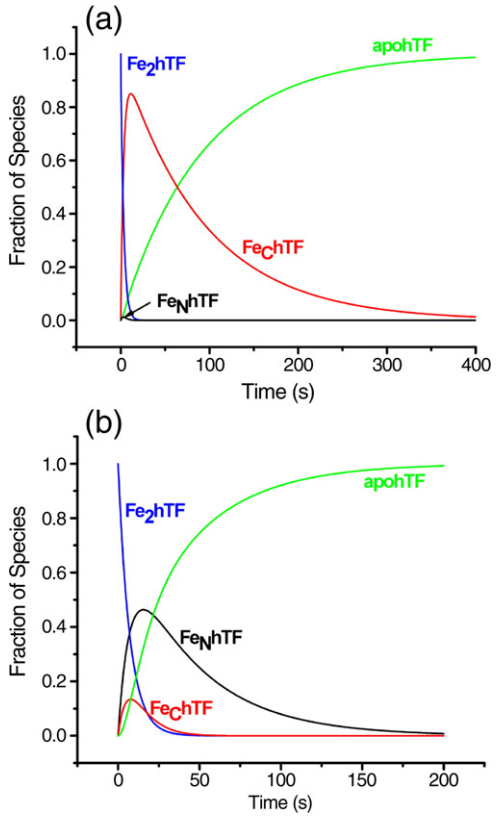

Fig. 3. Species–time distributions in the absence and in the presence of the sTFR. Distribution curves were calculated using Eqs. (1)–(4) (Table 1), with the following rate constants: (a) $k_{1N}=17.7\ min^{-1}$, $k_{1C}=0.72\ min^{-1}$, $k_{2N}=24.8\ min^{-1}$, and $k_{2C}=0.65\ min^{-1}$; (b) $k_{1N}=2.8\ min^{-1}$, $k_{1C}=5.5\ min^{-1}$, $k_{2N}=1.4\ min^{-1}$, and $k_{2C}=7.2\ min^{-1}$.

Findings by Hemadi *et al.*[34] are at variance with our results and those of Bali and Aisen[30,31] in two significant ways. As previously noted, Hemadi *et al.*[34] reported that iron is released first from the N-lobe and then from the C-lobe both in the presence and in the absence of the full-length TFR and that the rates differ by ~1000-fold when hTF is bound to TFR. Our results convincingly demonstrate that, at pH 5.6, the order is *reversed* such that, in the presence of the TFR, iron is released first from the C-lobe and the rates are comparable for the two lobes. While the use of a detergent micelle employed to solubilize the full-length TFR from the placenta precludes a truly direct comparison of their results with ours, we have nevertheless attempted to find the origin of the discrepancy by carrying out stopped-flow measurements with Fe_2hTF under the conditions of their experiments [50 mM acetate and 200 mM KCl (pH 5.6) at 37 °C] with and without the sTFR. Significantly, with acetate as the competing ligand, we find only limited removal of iron from the protein at pH 5.6 in the absence of sTFR and essentially no removal in its presence (Fig. S4a

and b). Only when EDTA is added to the acetate buffer do we observe a rapid and complete iron removal. While the experimental protocol of Hemadi *et al.*[34] may be adequate for iron removal below a pH of 5, it does not appear to be effective at stripping iron from the protein at the physiological pH (pH 5.6) of the endosome. These observations raise a question as to the relevance of their findings to ours and those of Egan *et al.* and argue for the use of a stronger chelator in these studies.

Salt-induced changes in rate constants

In the absence of the receptor, salt has the most dramatic effect (~4-fold) on the rate of iron release (k_1) from the N-lobes of Fe_2hTF and Fe_NhTF, increasing the rate constant from ~6 min^{-1} to ~27 min^{-1} (Fig. 4a). More modest changes (<2-fold) are seen for iron release from the N-lobe of $Lock_C$hTF and the isolated N-lobe (Fig. 4a), as well as from the C-lobe, and for other kinetic events in both lobes (data not shown). The rate constants for iron release (k_1) from the N-lobe of Fe_2hTF, Fe_NhTF, and $Lock_C$hTF increase linearly with increasing concentrations of salt between 50 mM and 600 mM KCl, presumably due, in large part, to Cl^- binding to the KISAB sites.[18,19] Of interest, iron release from the isolated N-lobe shows a very modest increase between 50 mM and 300 mM KCl and then decreases at 600 mM KCl. This is not observed for any of the other constructs, indicating that iron release from the isolated N-lobe is actually inhibited at a sufficiently high concentration of salt (even at pH 5.6). Nevertheless, iron release from the isolated N-lobe (at all salt concentrations) is significantly faster than iron release from the N-lobe of any of the full-length constructs at the same salt concentration, again consistent with the contention that the presence of the C-lobe slows iron release from the N-lobe. Of further interest is the observation that at 150 mM salt or below, the Fe_NhTF data fit well to the A→B→C model, whereas above 150 mM salt, the A→B→C→D model is required. Although this reveals that a new conformational event is observed with increasing concentrations of salt, the rate constant k_2=5.8 min^{-1} derived for this event is unchanged by increasing the salt concentration further.

Although salt is necessary for iron removal from the hTF/sTFR complexes,[32] the effect of the sTFR far exceeds that of salt. Thus, as indicated above, the sTFR induces a switch in the order of iron removal, which results in an increase in the rate constant for iron release from the C-lobe and a decrease in the rate constant for iron release from the N-lobe. Varying the concentration of salt when monitoring iron release from hTF/sTFR complexes results in more subtle changes in rate constants compared to the changes observed when the sTFR is absent (Fig. 4b). In both Fe_NhTF/sTFR and Fe_ChTF/sTFR complexes, iron release is preceded by a conformational change with a rate constant k_1 (Fig. 2b) that is affected by salt in opposite ways for the two constructs. As shown in Fig. 4b, for Fe_NhTF/sTFR, the rate constant k_1 *decreases* with increasing salt concentration from 37.1±1.1 min^{-1} to 16.4±1.1 min^{-1} and, for Fe_ChTF/sTFR, this event is only observed at 150 mM KCl and above, where k_1 *increases* from 9.4±0.2 min^{-1} to 20.3±1.1 min^{-1} with increasing salt concentration, making the rate constants for the N-lobe and the C-lobe more equal. In combination with the presence of the sTFR, this salt-sensitive conformational change appears to prime each lobe for iron release, perhaps through a KISAB mechanism.

In summary, we have assigned the specific events describing the iron release process from Fe_2hTF by

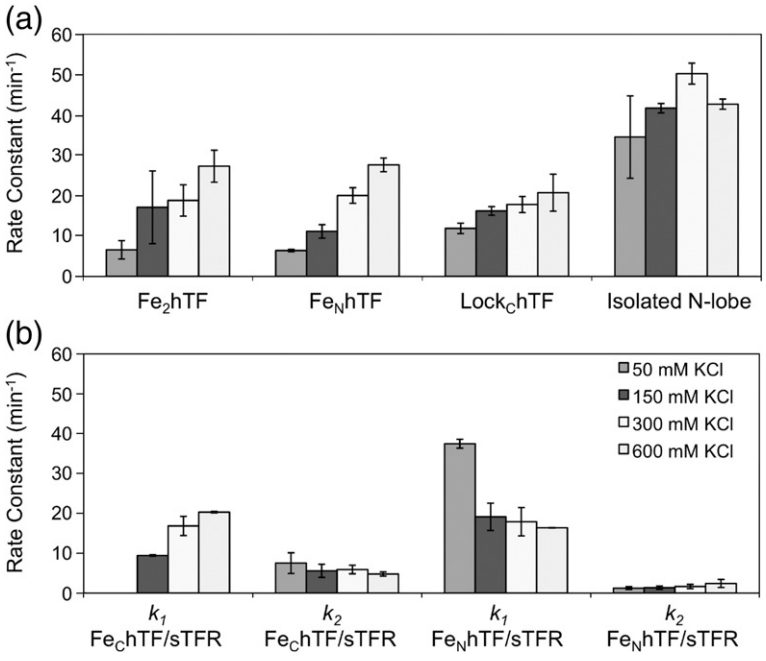

Fig. 4. Salt effect on iron release from various hTF constructs in the absence and in the presence of the sTFR. (a) Only the rate constant for iron release from the N-lobe at the various salt concentrations [indicated in the legend to (b)] is shown for Fe_2hTF, Fe_NhTF, $Lock_C$hTF, and the isolated N-lobe at pH 5.6. Except for the salt concentration, the conditions are exactly as indicated in the legend to Fig. 1. (b) Both k_1 and k_2, as a function of salt concentration, are presented for the two monoferric hTF species bound to the sTFR under the same conditions described above.

utilizing authentic monoferric and locked constructs to elucidate individual steps leading to complete iron removal in the absence and in the presence of the sTFR. The excellent signal-to-noise ratio in the kinetic curves for transferrin is unprecedented, allowing precise dissection of the kinetic events. At pH 5.6, the sTFR enhances the rate of iron release from the C-lobe (7-fold to 11-fold) and slows the rate of iron release from the N-lobe (6-fold to15-fold), making them more equivalent and producing an increase in the net rate of iron removal from Fe_2hTF. Additionally, the presence of the C-lobe in the protein slows iron release from the N-lobe and, along with the requirement of both lobes for strong binding to the receptor, provides a compelling argument for the bilobal nature of hTF. The unique combination of pH and salt-induced conformational changes in each lobe of hTF and the TFR appears to be exquisitely tuned to maximize the delivery of iron within the cell in the physiologically relevant time frame of 2 min.

Materials and Methods

Materials

Dulbecco's modified Eagle's medium–Ham F-12 nutrient mixture (DMEM–F12), antibiotic–antimycotic solution (100×), and trypsin solution were obtained from the GIBCO-BRL Life Technologies Division of Invitrogen. Fetal bovine serum was obtained from Atlanta Biologicals (Norcross, GA). Ultroser G (UG) was a serum replacement obtained from Pall BioSepra (Cergy, France). Ni-NTA resin was obtained from Qiagen. Corning-expanded surface roller bottles were obtained from Fisher Scientific, Hi-Prep 26/60 Sephacryl S-200HR and S-300HR prepoured columns were obtained from Amersham Pharmacia, and Amicon Ultra-4 (30 kDa cutoff) ultrafiltration concentrators were obtained from Millipore.

Protein production and purification

The DNA manipulations used to generate Fe_2hTF, Fe_NhTF, Fe_ChTF, $Lock_N$hTF, $Lock_C$hTF, and sTFR have been described in detail previously.[17,37,41] Briefly, for the production of recombinant hTF, baby hamster kidney (BHK) cells transfected with the pNUT plasmid containing the appropriate cDNA sequence are placed into two to four expanded surface roller bottles. Adherent BHK cells are grown in DMEM–F12 containing 10% fetal bovine serum. This medium was changed twice at 2-day intervals, after which DMEM–F12 containing the serum substitute UG (1%) and 1 mM butyric acid was used instead. UG and butyric acid have both been shown to increase the production of recombinant hTF and sTFR from BHK cells.[41] The amount of protein produced was usually determined using a competitive immunoassay.[42] The hexa-His-tagged recombinant protein from the tissue culture medium is captured by passage over a Ni-NTA column, followed by final purification on a gel-filtration column (S-200HR for hTF constructs and S-300HR for sTFR). Polyacrylamide gel electrophoresis in the presence of SDS was used to verify the homogeneity of all of the recombinant hTFs that were brought to a nominal concentration of 15 mg/mL. An accurate absorption coefficient for each construct was determined by a recently reported modified Edelhoch method.[43]

hTF/sTFR complexes are prepared by combining the sTFR with a small molar excess of hTF (Fe_2hTF, Fe_NhTF, Fe_ChTF, $Lock_N$hTF, and $Lock_C$hTF) and isolated by passage over an S-300HR column.[17] Complexes were adjusted to a nominal concentration of 15 mg/mL with respect to hTF.

Iron release kinetics

The kinetics of iron release from all of the hTF constructs, in the absence and in the presence of the sTFR, were monitored at pH 5.6 and 25 °C on an Applied Photophysics SX18.MV stopped-flow spectrofluorimeter.[17] One syringe contained protein (375 nM) in 300 mM KCl, and the other syringe contained 200 mM Mes buffer (pH 5.6), 300 mM KCl, and 8 mM EDTA (our "standard" conditions). Samples were excited at 280 nm, and fluorescence emission was monitored using a high-pass 320-nm cut-on filter. For KCl titrations, one syringe contained protein in either 50 mM, 150 mM, 300 mM, or 600 mM KCl; the other contained 200 mM Mes buffer (pH 5.6), 8 mM EDTA, and an equivalent concentration of KCl. Rate constants were determined by fitting the change in fluorescence intensity *versus* time to the appropriate model using Origin software (version 7.5). The equations used to fit the data are provided in Results and Discussion and Supplemental Data, which also contain their complete derivation and program code for Origin. These equations provide more precise and accurate rate constants than the exponential equations used in our previous work.[26,27,44] Nevertheless, the rate constants that were previously reported are within the standard deviations of the current values. All iron release curves shown in Fig. 1 are an average of at least 4 (with a maximum of 32) separate experiments performed on different days and have all been normalized to a fluorescence intensity of 1.0 at the end of the iron release reaction. Reported rate constants are averages from the curve fitting of data obtained on multiple days with two or more protein preparations. A direct measurement of the kinetics of iron release using the stopped-flow absorbance spectrophotometry at ~465 nm is difficult because of the low intensity of the band and the limited solubility of the receptor.[26] Therefore, assignment of rate constants to iron release events (as opposed to conformational changes) was accomplished by comparing rate constants among the different constructs. The rate constants for iron removal from a given lobe are expected to be very similar across constructs and, hence, readily identified. That proved to be the case, as shown by the rate constant assignments in Table S1.

Acknowledgements

This work was supported by U.S. Public Health Service grant R01-DK-21739 from the National Institute of Diabetes and Digestive and Kidney Diseases (A.B.M.) and grant R01-GM-20194 from the National Institute of General Medical Sciences (N.D.C.). Support for S.L.B. and A.N.S. came from Hemostasis and Thrombosis Training grant 5T32HL007594 issued to Dr. Kenneth G. Mann at The University of Vermont by the National Heart,

Lung, and Blood Institute. We thank Dr. Nicholas G. James for technical assistance with some of the stopped-flow experiments and Dr. Stephen J. Everse for his help with the preparation of some of the figures.

Supplementary Data

Supplementary data associated with this article can be found, in the online version, at doi:10.1016/j.jmb.2009.11.023

References

1. Hall, D. R., Hadden, J. M., Leonard, G. A., Bailey, S., Neu, M., Winn, M. & Lindley, P. F. (2002). The crystal and molecular structures of diferric porcine and rabbit serum transferrins at resolutions of 2.15 and 2.60 Å, respectively. *Acta Crystallogr., Sect. D: Biol. Crystallogr.* **58**, 70–80.
2. Wally, J., Halbrooks, P. J., Vonrhein, C., Rould, M. A., Everse, S. J., Mason, A. B. & Buchanan, S. K. (2006). The crystal structure of iron-free human serum transferrin provides insight into inter-lobe communication and receptor binding. *J. Biol. Chem.* **281**, 24934–24944.
3. Mason, A. B., Halbrooks, P. J., James, N. G., Connolly, S. A., Larouche, J. R., Smith, V. C. *et al.* (2005). Mutational analysis of C-lobe ligands of human serum transferrin: insights into the mechanism of iron release. *Biochemistry*, **44**, 8013–8021.
4. Dautry-Varsat, A., Ciechanover, A. & Lodish, H. F. (1983). pH and the recycling of transferrin during receptor-mediated endocytosis. *Proc. Natl Acad. Sci. USA*, **80**, 2258–2262.
5. Klausner, R. D., Van Renswoude, J., Ashwell, G., Kempf, C., Schechter, A. N., Dean, A. & Bridges, K. R. (1983). Receptor-mediated endocytosis of transferrin in K562 cells. *J. Biol. Chem.* **258**, 4715–4724.
6. Aisen, P., Enns, C. & Wessling-Resnick, M. (2001). Chemistry and biology of eukaryotic iron metabolism. *Int. J. Biochem. Cell Biol.* **33**, 940–959.
7. Ohgami, R. S., Campagna, D. R., Greer, E. L., Antiochos, B., McDonald, A., Chen, J. *et al.* (2005). Identification of a ferrireductase required for efficient transferrin-dependent iron uptake in erythroid cells. *Nat. Genet.* **37**, 1264–1269.
8. Dhungana, S., Taboy, C. H., Zak, O., Larvie, M., Crumbliss, A. L. & Aisen, P. (2004). Redox properties of human transferrin bound to its receptor. *Biochemistry*, **43**, 205–209.
9. Sendamarai, A. K., Ohgami, R. S., Fleming, M. D. & Lawrence, C. M. (2008). Structure of the membrane proximal oxidoreductase domain of human Steap3, the dominant ferrireductase of the erythroid transferrin cycle. *Proc. Natl Acad. Sci. USA*, **105**, 7410–7415.
10. Anderson, B. F., Baker, H. M., Dodson, E. J., Norris, G. E., Rumball, S. V., Waters, J. M. & Baker, E. N. (1987). Structure of human lactoferrin at 3.2-Å resolution. *Proc. Natl Acad. Sci. USA*, **84**, 1769–1773.
11. Baker, H. M., Anderson, B. F., Brodie, A. M., Shongwe, M. S., Smith, C. A. & Baker, E. N. (1996). Anion binding by transferrins: importance of second-shell effects revealed by the crystal structure of oxalate-substituted diferric lactoferrin. *Biochemistry*, **35**, 9007–9013.
12. MacGillivray, R. T., Moore, S. A., Chen, J., Anderson, B. F., Baker, H., Luo, Y. *et al.* (1998). Two high-resolution crystal structures of the recombinant N-lobe of human transferrin reveal a structural change implicated in iron release. *Biochemistry*, **37**, 7919–7928.
13. Jeffrey, P. D., Bewley, M. C., MacGillivray, R. T., Mason, A. B., Woodworth, R. C. & Baker, E. N. (1998). Ligand-induced conformational change in transferrins: crystal structure of the open form of the N-terminal half-molecule of human transferrin. *Biochemistry*, **37**, 13978–13986.
14. Dewan, J. C., Mikami, B., Hirose, M. & Sacchettini, J. C. (1993). Structural evidence for a pH-sensitive dilysine trigger in the hen ovotransferrin N-lobe: implications for transferrin iron release. *Biochemistry*, **32**, 11963–11968.
15. Halbrooks, P. J., He, Q. Y., Briggs, S. K., Everse, S. J., Smith, V. C., MacGillivray, R. T. & Mason, A. B. (2003). Investigation of the mechanism of iron release from the C-lobe of human serum transferrin: mutational analysis of the role of a pH sensitive triad. *Biochemistry*, **42**, 3701–3707.
16. Halbrooks, P. J., Giannetti, A. M., Klein, J. S., Bjorkman, P. J., Larouche, J. R., Smith, V. C. *et al.* (2005). Composition of pH-sensitive triad in C-lobe of human serum transferrin. Comparison to sequences of ovotransferrin and lactoferrin provides insight into functional differences in iron release. *Biochemistry*, **44**, 15451–15460.
17. Byrne, S. L., Leverence, R., Klein, J. S., Giannetti, A. M., Smith, V. C., MacGillivray, R. T. *et al.* (2006). Effect of glycosylation on the function of a soluble, recombinant form of the transferrin receptor. *Biochemistry*, **45**, 6663–66673.
18. Kretchmar, S. A. & Raymond, K. N. (1988). Effects of ionic strength on iron removal from the monoferric transferrins. *Inorg. Chem.* **27**, 1436–1441.
19. Marques, H. M., Watson, D. L. & Egan, T. J. (1991). Kinetics of iron removal from human serum monoferric transferrins by citrate. *Inorg. Chem.* **30**, 3758–3762.
20. Harris, W. R. (1985). Thermodynamics of anion binding to human serum transferrin. *Biochemistry*, **24**, 7412–7418.
21. He, Q. Y. & Mason, A. B. (2002). Molecular aspects of release of iron from transferrin. In *Molecular and Cellular Iron Transport* (Templeton, D. M., ed.), Marcel Dekker, Inc., Toronto, Canada.
22. Lehrer, S. S. (1969). Fluorescence and absorption studies of the binding of copper and iron to transferrin. *J. Biol. Chem.* **244**, 3613–3617.
23. Gaber, B. P., Miskowski, V. & Spiro, T. G. (1974). Resonance Raman scattering from iron(III)- and copper(II)-transferrin and an iron(III) model compound. A spectroscopic interpretation of the transferrin binding site. *J. Am. Chem. Soc.* **96**, 6868–6873.
24. Chen, Y. & Barkley, M. D. (1998). Toward understanding tryptophan fluorescence in proteins. *Biochemistry*, **37**, 9976–9982.
25. Vivian, J. T. & Callis, P. R. (2001). Mechanisms of tryptophan fluorescence shifts in proteins. *Biophys. J.* **80**, 2093–2109.
26. James, N. G., Berger, C. L., Byrne, S. L., Smith, V. C., Macgillivray, R. T. & Mason, A. B. (2007). Intrinsic fluorescence reports a global conformational change in the N-lobe of human serum transferrin following iron release. *Biochemistry*, **46**, 10603–10611.
27. James, N. G., Byrne, S. L., Steere, A. N., Smith, V. C., MacGillivray, R. T. A. & Mason, A. B. (2009). Inequivalent contribution of the five tryptophan residues in the C-lobe of human serum transferrin to

the fluorescence increase when iron is released. *Biochemistry*, **48**, 2858–2867.
28. James, N. G., Byrne, S. L. & Mason, A. B. (2009). Incorporation of 5-hydroxytryptophan into transferrin and its receptor allows assignment of the pH induced changes in intrinsic fluorescence when iron is released. *Biochim. Biophys. Acta*, **1794**, 532–540.
29. Bali, P. K., Zak, O. & Aisen, P. (1991). A new role for the transferrin receptor in the release of iron from transferrin. *Biochemistry*, **30**, 324–328.
30. Bali, P. K. & Aisen, P. (1991). Receptor-modulated iron release from transferrin: differential effects on N- and C-terminal sites. *Biochemistry*, **30**, 9947–9952.
31. Bali, P. K. & Aisen, P. (1992). Receptor-induced switch in site–site cooperativity during iron release by transferrin. *Biochemistry*, **31**, 3963–3967.
32. Egan, T. J., Zak, O. & Aisen, P. (1993). The anion requirement for iron release from transferrin is preserved in the receptor–transferrin complex. *Biochemistry*, **32**, 8162–8167.
33. el Hage Chahine, J. M. & Pakdaman, R. (1995). Transferrin, a mechanism for iron release. *Eur. J. Biochem.* **230**, 1102–1110.
34. Hemadi, M., Ha-Duong, N. T. & el Hage Chahine, J. M. (2006). The mechanism of iron release from the transferrin–receptor 1 adduct. *J. Mol. Biol.* **358**, 1125–1136.
35. Harris, W. R., Bali, P. K. & Crowley, M. M. (1992). Kinetics of iron removal from monoferric and cobalt-labeled monoferric transferrins by diethylenetriaminepenta(methylenephosphonic acid) and diethylenetriaminepentaacetic acid. *Inorg. Chem.* **31**, 2700–2705.
36. Mason, A. B. & Everse, S. J. (2008). Iron transport by transferrin. In *Iron Metabolism and Disease* (Fuchs, H., ed.), Research Signpost, Kerala, India.
37. Byrne, S. L. & Mason, A. B. (2009). Human serum transferrin: a tale of two lobes. Urea gel and steady state fluorescence analysis of recombinant transferrins as a function of pH, time, and the soluble portion of the transferrin receptor. *J. Biol. Inorg. Chem.* **14**, 771–781.
38. Mason, A. B., Tam, B. M., Woodworth, R. C., Oliver, R. W., Green, B. N., Lin, L. N. *et al.* (1997). Receptor recognition sites reside in both lobes of human serum transferrin. *Biochem. J.* **326**, 77–85.
39. Zak, O., Trinder, D. & Aisen, P. (1994). Primary receptor-recognition site of human transferrin is in the C-terminal lobe. *J. Biol. Chem.* **269**, 7110–7114.
40. Giannetti, A. M., Snow, P. M., Zak, O. & Bjorkman, P. J. (2003). Mechanism for multiple ligand recognition by the human transferrin receptor. *PLoS Biol.* **1**, E51.
41. Mason, A. B., Halbrooks, P. J., Larouche, J. R., Briggs, S. K., Moffett, M. L., Ramsey, J. E. *et al.* (2004). Expression, purification, and characterization of authentic monoferric and apo-human serum transferrins. *Protein Expression Purif.* **36**, 318–326.
42. Mason, A. B., He, Q. Y., Adams, T. E., Gumerov, D. R., Kaltashov, I. A., Nguyen, V. & MacGillivray, R. T. (2001). Expression, purification, and characterization of recombinant nonglycosylated human serum transferrin containing a C-terminal hexahistidine tag. *Protein Expression Purif.* **23**, 142–150.
43. James, N. G. & Mason, A. B. (2008). Protocol to determine accurate absorption coefficients for iron-containing transferrins. *Anal. Biochem.* **378**, 202–207.
44. Mason, A. B., Halbrooks, P. J., James, N. G., Byrne, S. L., Grady, J. K., Chasteen, N. D. *et al.* (2009). Structural and functional consequences of the substitution of glycine 65 with arginine in the N-lobe of human transferrin. *Biochemistry*, **48**, 1945–1953.